
STRUCTURE, PHASE TRANSFORMATIONS,
AND DIFFUSION

Investigation of Cyclic Oxidation Behavior of (Cr, Mo, Si)-Containing ($\alpha_2 + \gamma$) TiAl-Based Alloys Synthesized by ECAS Sintering

Y. Garip^a and O. Ozdemir^{a, *}

^a*Sakarya Applied Science University, Technology Faculty, Department of Metallurgy and Materials Engineering,
Esentepe Campus, Sakarya, 54187 Turkey*

**e-mail: oozdemir@sakarya.edu.tr*

Received February 26, 2019; revised April 16, 2019; accepted October 22, 2019

Abstract—Ti–48Al–2Cr–2Mo–(0 and 0.5 at %) Si intermetallic alloys were synthesized by electric current-assisted sintering (ECAS). Microstructures of the alloys were characterized using scanning electron microscopy (SEM), electron diffraction spectroscopy (EDS), and X-ray diffraction (XRD) methods of analysis. It was found that the microstructures of the produced alloys consist of α_2 -Ti₃Al and γ -TiAl phases. The cycle oxidation behaviors of the alloys were carried out between 700 and 900°C temperatures for 180 h in air. The oxide scale has comprised the TiO₂ and Al₂O₃ mixture layer, intermediate Al₂O₃ layer, and outermost TiO₂ layer. The oxidation rate constants and activation energies of the alloys were calculated.

Keywords: TiAl intermetallic, oxidation, powder metallurgy, ECAS

DOI: 10.1134/S0031918X20040043

INTRODUCTION

TiAl based alloys have been regarded as a candidate material for high-temperature applications due to its superior properties, such as low density, high temperature strength, high elastic modulus, high melting temperature, creep resistance, and relatively good oxidation resistance. The combination of these properties makes TiAl alloys attractive for high-temperature applications, such as aviation gas turbines and automotive engine components [1–3]. Titanium-based alloys make up one-third of the weight of airplane engines and are the second most employed materials used in engine parts after nickel based superalloys [4]. Furthermore, these materials are considered as significant potential substitutes for nickel-based superalloys [4]. However, the application of these alloys is restricted because of poor room-temperature ductility, creep resistance, and inadequate oxidation resistance at temperatures higher than 800°C [3, 5]. Alloying elements of Nb, Ta, Mo, W, and Si provide an important contribution to increasing the oxidation resistance of TiAl based alloys [4, 6, 7]. The improvement of the oxidation resistance is generally explained through the doping effect and an increase in Al diffusivity and activity. The doping effect is attributed to a reduction of oxygen vacancy concentration and diffusion of oxygen [6].

The electric current-assisted sintering (ECAS) process is a consolidation or synthesis process in which the mechanical pressure is applied together

with electric current passing through loose powders placed in a die or a cold formed compact. Heat is yielded by the Joule effect that takes place in consequence of the electric current passing through a resistive material. Furthermore, the ECAS method has several superior features compared to traditional sintering methods, such as hot pressing or pressureless sintering. This method has many advantages, including lower processing temperature, shorter sintering time, faster heating rate, the elimination of the need of sintering aids, lesser sensitivity to the feature of the starting powders and the synthesized materials have a density close to theoretical density [8–10]. The aim of this study was to determine the effect of ECAS method on the cycle oxidation behavior of TiAl based alloys containing small addition of Si. Therefore, cyclic oxidation behavior of Ti–48Al–2Cr–2Mo and Ti–48Al–2Cr–2Mo–0.5Si at % intermetallic alloys was investigated in air at temperatures ranging from 700 to 900°C and exposure for 180 h.

EXPERIMENTAL DETAILS

Materials Preparation

The TiAl-based intermetallics with a nominal composition of Ti–48Al–2Cr–2Mo and Ti–48Al–2Cr–2Mo–0.5Si (at %) were synthesized by electric current-assisted sintering (ECAS) technique. The powders contain titanium (99.5%, particulate size 40 μm), aluminum (99.5%, size 10 μm), chromium

(99.8%, size 5 μm) molybdenum (99.9%, size 3 μm), and silicon (99.9%, size 5 μm). The weight of each powder was measured by an electronic balance.

In order to obtain a homogenous powder mixture, the powders were milled by in a stainless steel container with stainless steel balls. The rotation speed of ball milling was 200 rpm, milling exposure was 4 h, and the mass ratio of balls to powders was 5 : 1. Then 6 g of a mixture of powders were filled in a steel die with a 20 mm internal diameter. The mixture of powders was compacted in the steel die by an under uniaxial pressure of 60 MPa for 1 min. The compact was synthesized by application of a sintering pressure of 80 MPa at an electric current of 4200 A for 35 min in the air via ECAS. The sintering pressure was kept up to the end of the operation. After the synthesizing, the specimen inside the steel die was removed using uniaxial pressure and cooled to room temperature.

Cyclic Oxidation Test

Before cyclic oxidation test, the original surface area of each specimens was attested using the Solidworks and then weighed by the electronic balance with an accuracy of 0.01 mg. The oxidation tests were conducted in a resistance furnace at 700, 800, and 900°C for 180 h. Oxidation test was performed in the air up to 15 cycles and each cycle consisted of heating the specimens to test temperature, waiting for 12 h at that temperature and then cooled down to ambient temperature in air. The weight changes after each cycle of oxidation was weighed using an electronic balance with 0.01 mg sensitivity. Furthermore, two measurements were carried out for each cycle, with results averaged and after that recorded. Afterwards the specimens were re-placed to the furnace for exposure again. The procedure was repeated up to the end of the cycle oxidation test.

Characterization

The present phases of the specimens after the oxidation were identified by X-ray diffraction (XRD, RIGAKU) analysis using Cu $K\alpha$ radiation at 40 kV and current of 40 mA. Data were scanned in the 2θ range from 10° to 90°. The surface and the cross-section morphologies of the oxidation products were characterized by a scanning electron microscope (SEM, JEOL) and the microanalysis was carried out by an energy dispersive spectroscopy (EDS). After oxidation test, the weight change per unit area (ΔW) was evaluated as following:

$$\Delta W = \Delta m / A, \quad (1)$$

where ΔW is the weight change per unit area (mg cm^{-2}), Δm is the weight change, A is the surface area of a specimen (cm^2).

RESULTS AND DISCUSSION

Oxidation Behaviors

The cyclic oxidation kinetics of the Ti–8Al–2Cr–2Mo and Ti–48Al–2Cr–2Mo–0.5Si at % alloys were studied in air at 700, 800, and 900°C for 180 h. The kinetics of oxidation of the alloys was determined as a function time-based on the weight change per unit area and the results are shown in Figs. 1a–1c. As shown in Figs. 1a–1c, the weight changes of the TiAl-based alloys were increased as the temperature increased. The oxidation temperature had a significant effect on the weight changes of the alloys, since it increased the oxidation rate. After exposure for 180 h at 700, 800, and 900°C, the total weight change in the alloys was about 1.4, 2.1, and 7.8 mg cm^{-2} for Ti–48Al–2Cr–2Mo alloy and 0.85, 1.3, and 3.6 mg cm^{-2} for Ti–48Al–2Cr–2Mo–0.5Si alloy, respectively. The weight changes for both alloys at 700°C were less than 1.4 mg cm^{-2} , which means that oxidation is not severe at this temperature. At all test temperatures, it was seen that the weight change of the alloy with Si addition was about 2 times less than that of the alloys without Si. It is seen that cycle oxidation resistance of the alloys increases with the addition of Si. The beneficial effect of Si addition was also observed on the other TiAl-based intermetallics [11, 12]. The alloys were observed to oxidize rapidly at the early stages of oxidation at each test temperature. This may be interpreted by the adsorption of oxygen from the atmosphere followed by nucleation and growth of oxides in the early stage due to that the Ti and Al have high affinity to oxygen. As oxidation proceeds, the observed decrease in the oxidation rate suggests that an alumina-rich layer began to control the oxidation. Since diffusion and reaction rates increased with the increase of the oxidation temperature, a significant weight change was observed in the alloys, especially at 900°C (Fig. 1c). Furthermore, no spallation occurred on the oxidation scale of the alloys during the cycle oxidation test at 700–900°C. The oxidation kinetics of the alloys was evaluated by fitting the weight changes to the following equation [13]:

$$\Delta W = k_p t^n, \quad (2)$$

where ΔW is the weight change per unit of surface area, k_p is the oxidation rate constant ($\text{mg cm}^{-2} \text{h}^{-n}$), and t is the exposure time (h), and n is the power exponent that represents the law of oxide growth kinetics. The weight changes versus the square root of time for the alloys are shown in Figs. 1a–1c. The oxidation kinetic curves were nearly linear at 700, 800, and 900°C, showing that the oxidation process follows a parabolic rate law ($n = 0.5$). In Wagner's theory, the parabolic rate constant can be described as a function of the outward diffusion of the metal ions or of the inward diffusion of the oxygen through the oxide scale and the slowest diffusion through the oxide scale is the rate-limiting step in the overall oxidation process [13]. The linear regression analysis of the weight change versus time plot was carried out based on the Eq. (4)

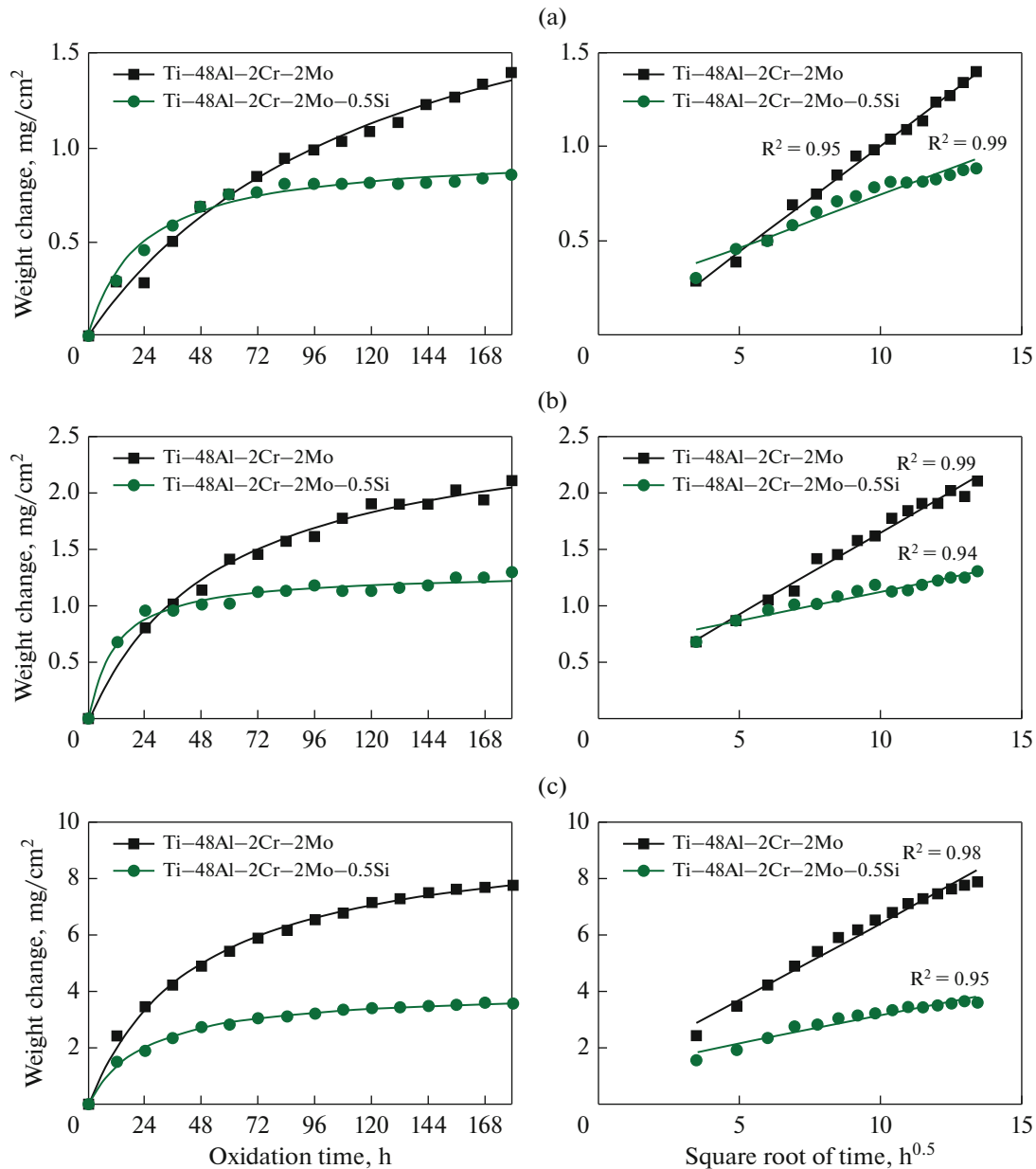


Fig. 1. Plots of weight change vs. oxidation time and weight change vs. the square root of oxidation time, recorded after oxidation of Ti-48Al-2Cr-2Mo and Ti-48Al-2Cr-2Mo-0.5Si alloys for 180 h, (a) 700, (b) 800, and (c) 900°C.

using GraphPad Prism 7 program soft and the slope of the best-fit line would yield oxidation rate constant values of the alloys. As is shown in Table 1, the k_p val-

Table 1. Oxidation rate constant (k_p , mg cm⁻² h^{-0.5}) values of the alloys for 180 h

T , °C	Ti-48Al-2Cr-2Mo	Ti-48Al-2Cr-2Mo-0.5Si
700	0.01087	0.00356
800	0.01857	0.00669
900	0.33315	0.06677

ues of the alloys increase with the increase of temperature. This means that higher oxidation rate constant value reflects a higher oxidation rate. It was found that oxidation rate constant decreases with the addition of Si, suggesting that Si has a beneficial effect on developing the oxidation resistance of the alloys.

The oxidation rate constant (k_p) is a function of reaction temperature and it can be defined by the Arrhenius equation:

$$k_p = k_0 \exp(-Q/RT), \quad (3)$$

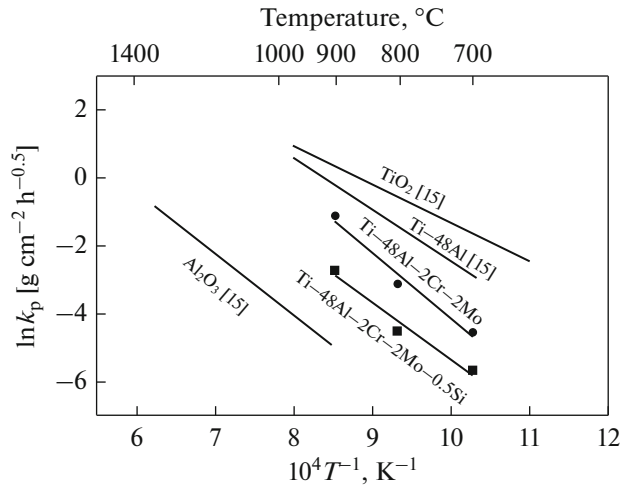


Fig. 2. Oxide forming kinetics of Ti-48Al-2Cr-2Mo and Ti-48Al-2Cr-2Mo-0.5Si alloys with the previously published data superimposed.

where k_0 is a constant, Q is the activation energy, R is the gas constant (8.314 J/(mol K)) and T is temperature (K). Taking the natural logarithm from both sides of Eq. (5) yields:

$$\ln(k_p) = \ln(k_0) - (Q/RT). \quad (4)$$

The oxidation rate constant (k_p) values of our alloys were compared with previously published data, as shown in Fig. 2. It can be seen that the k_p values of Ti-48Al-2Cr-2Mo and Ti-48Al-2Cr-2Mo-0.5Si alloys were located between the alumina and TiO₂ forming kinetics. The values of activation energy can be calculated by knowing the slope of the linear regression line of $\ln(k_p)$ vs. T^{-1} plot. The activation energy values of our alloys and TiAl-based alloys obtained from the literature are presented in Table 2. The activation energy values of the Ti-48Al-2Cr-2Mo and Ti-48Al-2Cr-2Mo-0.5Si alloys were smaller than that of Ti-45.9Al-8Nb alloy but (were) bigger than those of Ti-48Al-2Cr-2Nb and Ti-48Al-2Cr-2Nb-(0.5-1)W alloys. This may be caused by oxidation temperature, type of atmosphere, alloy's initial microstructure, effect of alloying elements, and surface finishing.

Table 2. Activation energies of oxidation for TiAl-based alloys

Alloy	Reference	Q , kJ mol ⁻¹
Ti-48Al-2Cr-2Mo	[this study]	160
Ti-48Al-2Cr-2Mo-0.5Si	[this study]	137
Ti-45.9Al-8Nb	[14]	200
Ti-48Al-2Cr-2Nb	[15]	138
Ti-48Al-2Cr-2Nb-0.5W	[15]	114
Ti-48Al-2Cr-2Nb-1W	[15]	146

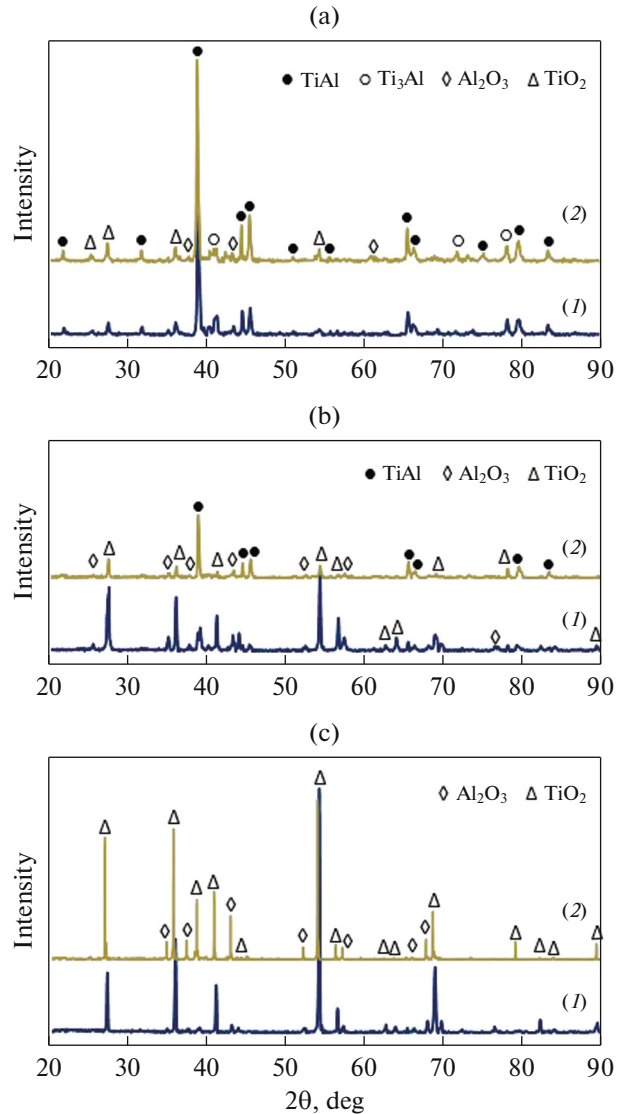


Fig. 3. XRD patterns of the oxidized TiAl-based alloys for 180 h: (a) 700, (b) 800, and (c) 900°C, (1) Ti-48Al-2Cr-2Mo, (2) Ti-48Al-2Cr-2Mo-0.5Si at %.

Composition and Morphology of Oxide Products

Oxidation products were observed on all the surfaces of alloys exposed to 800 and 900°C. However, oxidation was not observed at 700°C. The results of XRD analysis of the Ti-48Al-2Cr-2Mo and Ti-48Al-2Cr-2Mo-0.5Si at % alloys after oxidation at 700, 800, and 900°C for 180 h are shown in Figs. 3a-3c. It was determined by XRD that the surfaces of the oxidized alloys have consisted of TiO₂ and Al₂O₃ at all test temperatures after exposure for 180 h. Since the formed oxide scale was not thick or uniform, the TiAl and Ti₃Al phases were observed. After exposure to 700°C, the Ti₃Al phase was detected and identified, but it was not detected at 800 and 900°C in the XRD patterns. This was most likely caused by Ti₃Al oxidized to TiO₂.

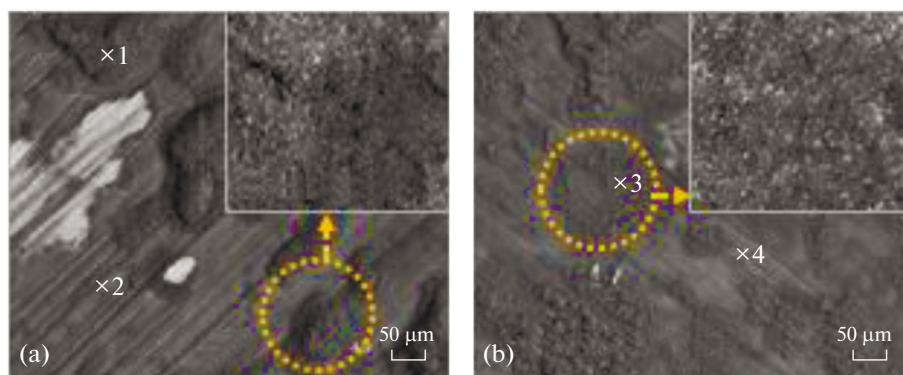


Fig. 4. SEM surface morphologies of oxidized alloys at 700°C for 180 h (a) Ti–48Al–2Cr–2Mo and (b) Ti–48Al–2Cr–2Mo–0.5Si (at %) with EDS analysis in marked points. Insets show details of the oxides.

with increasing temperature. At 800°C, the intensity of the TiO_2 and Al_2O_3 phases increased, while the intensity of the TiAl phase decreased, which means that the oxide scale thickness increases with temperature. It is shown in Fig. 3c that the oxide scale formed in both alloys at 900°C was composed of TiO_2 and Al_2O_3 phases. Due to the thick oxide scale, TiAl phase was not observed by the XRD.

Furthermore, the oxides of alloying elements (Cr, Mo, and Si) were not observed due to their dissolution in the oxide scale. The Si oxides were not detected in the XRD patterns because of that the Si concentration in the alloy was insufficient to form a separate SiO_2 layer or SiO_2 islands in the oxide scale. The surface morphologies of the oxidized alloys at 700°C exposure for 180 h are shown in Fig. 4. It was seen in Figs. 4a and 4b that the images of the surfaces of the oxidized Ti–48Al–2Cr–2Mo and Ti–48Al–2Cr–2Mo–0.5Si (at %) alloys were composed of dark (marked as 1 and 3) and grey (marked as 2 and 4) phase regions. The chemical composition of these regions was determined by EDS analysis (Table 3) and these regions were composed of titanium, aluminum, and oxygen. It was seen from Table 3 that the O content of Al-rich regions (TiAl) was lower. Because the high solubility of oxygen in the α_2 - Ti_3Al phase, it is suggested that these phase regions are more rapidly oxidized than the γ -TiAl phase regions do [16]. Furthermore, this difference in oxidation rate is caused by the large difference in the Ti and

Al contents between the α_2 - Ti_3Al and γ -TiAl phases. As the Ti content in the α_2 - Ti_3Al phase is significantly larger than that in the γ -TiAl phase, the α_2 - Ti_3Al phase rapidly forms TiO_2 when exposed to high temperatures [17]. According to the XRD analysis results (Fig. 3), the Ti and Al oxides forming these regions were determined as the TiO_2 and Al_2O_3 phases. Moreover, it is seen in Fig. 4a that oxidation products formed on the surface of Ti–48Al–2Cr–2Mo alloy were more than that of the other alloy. As shown in Fig. 1a, this affected the kinetic curves of the oxidized alloys. The oxides (marked as 1), which are additionally formed on the surface of the alloy, were non-homogeneously distributed in clusters (Fig. 7a). Therefore, the surface of the alloy had an uneven morphology. A detailed SEM photograph of the cluster area is displayed in Fig. 4a. It can be seen that the cluster area has consisted of fine oxides with spherical crystals.

The surface of the oxidized Ti–48Al–2Cr–2Mo–0.5Si alloy was smoother than that of the alloy without Si (Fig. 4b). The higher magnification of the marked area showed that the alloy surface consisted of oxides with bar-shaped structures.

Considering that the oxide scale formed on the surfaces of TiAl-based intermetallics at high temperatures, after the early stage, the TiO_2 forms the outer oxide layer, since faster growing TiO_2 grains overgrow Al_2O_3 grains [17]. As seen from Figs. 5a, 5b, after exposure to 800 and 900°C, the surface morphologies of the alloys were completely different in comparison with 700°C and the alloys surfaces consisted of more oxide products. It was also observed that the oxide particles in some areas of surface grow faster than those of other areas and thus a non-uniform surface morphology forms. According to EDS analysis (Table 4) of the areas in which the fast developing oxide grains were marked as (×2) and (×3) in Figs. 5a and 5b, these grains formed from Ti oxide. However, the EDS analysis results of more slowly developing oxide areas (marked as ×1) showed that these areas were aluminum rich. As shown in the XRD patterns (Fig. 3b), the

Table 3. Chemical compositions (in at %) of oxide scales at marked points in Fig. 4

Points	Element					
	O	Ti	Al	Cr	Mo	Si
1	57.9	25.2	16.6	0.2	0.1	–
2	38.2	28.4	32.8	0.3	0.2	–
3	51.4	27.7	19.3	0.9	0.5	0.2
4	43.2	26.5	29.6	0.4	0.2	0.1

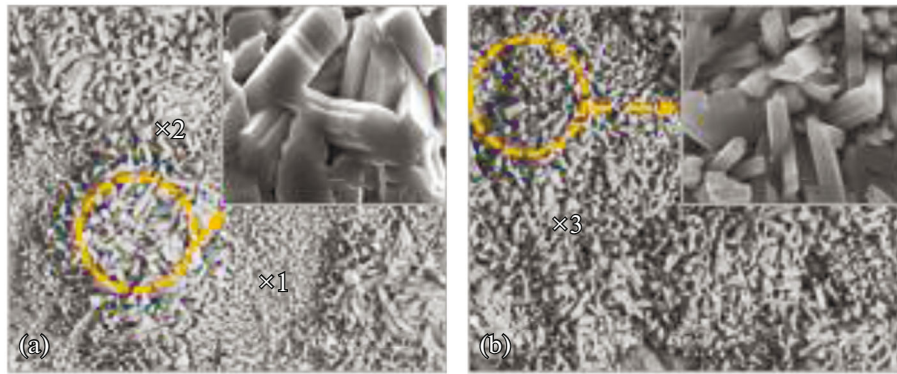


Fig. 5. SEM surface morphologies of oxidized alloys at 800°C for 180 h (a) Ti-48Al-2Cr-2Mo and (b) Ti-48Al-2Cr-2Mo-0.5Si (at %) with EDS analysis in marked points. Insets show details of the oxides.

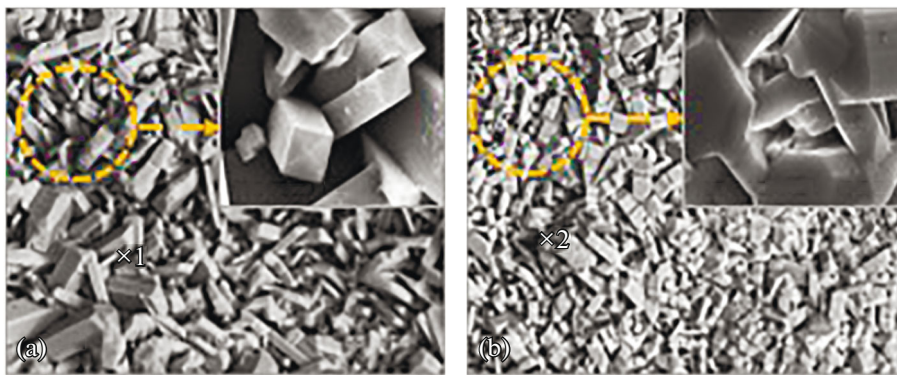


Fig. 6. SEM surface morphologies of oxidized alloys at 900°C for 180 h (a) Ti-48Al-2Cr-2Mo and (b) Ti-48Al-2Cr-2Mo-0.5Si (at %) with EDS analysis in marked points. Insets show details of the oxides.

aluminum and titanium oxides forming these areas were determined as Al₂O₃ and TiO₂.

Additionally, higher magnification of marked areas (Figs. 5a and 5b) shows that large-grained titanium oxide on the surface have had a polyhedron structure. As is shown in Figs. 6a and 6b, an increase in temperature to 900°C increased the oxidation rate, which also resulted in the formation of larger titanium oxide grains. After oxidation at 800 and 900°C, there was not observed an important difference in the surface morphology of the alloys, except for oxide grain size.

Similarly, titanium oxide grains formed at 900°C appear to have a pillar-like structure. Similar results were reported by many authors [15, 16, 18]. It can also be seen from SEM images at higher magnifications that an increase occurs in lateral growth of oxide particles at 900°C compared with the case of 800°C. The coverage of the surface with relatively larger Ti oxide grains at increased oxidation temperature results in an increase in TiO₂ peak intensity in the X-ray diffraction patterns (Fig. 3c).

Due to the fact that the Al₂O₃ layer was underneath the TiO₂ layer in oxide scale, the absence of significant

increase in Al₂O₃ peak intensity at 900°C can be attributed to the greater growth of titanium oxide grains compared with the case of 800°C. As is seen in Fig. 1c, the weight changes increased by the increase in exposure temperature. This result was in good agreement with the SEM examination.

Cross-Sectional Morphology

After exposure to oxidation at 900°C for 180 h, the cross-sectional microstructures of the alloys are shown in Fig. 7.

Table 4. Chemical compositions (in at %) of oxide scales at marked points in Fig. 5

Points	Element					
	O	Ti	Al	Cr	Mo	Si
1	52.3	14.1	32.8	0.6	0.2	—
2	65.1	33.3	1.4	0.1	0.1	—
3	63.7	33.6	2.1	0.3	0.2	0.1

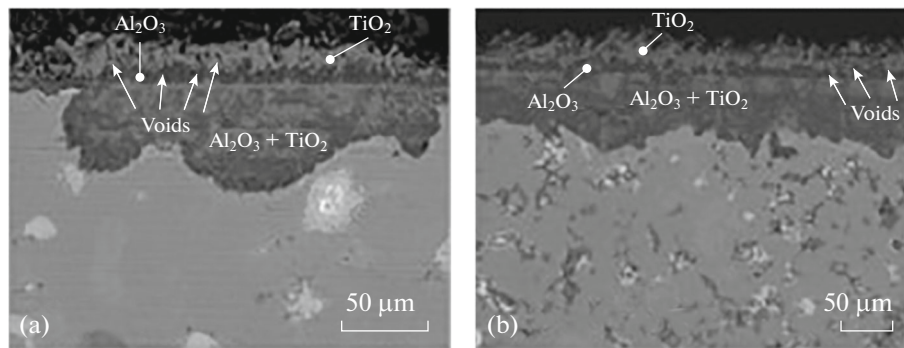


Fig. 7. SEM images of the cross-sectional microstructures of oxide scale formed on the alloys, after oxidation at 900°C for 180 h. (a) Ti-48Al-2Cr-2Mo and (b) Ti-48Al-2Cr-2Mo-0.5Si.

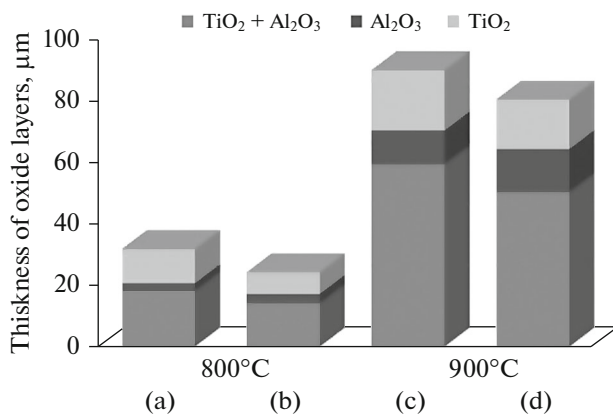


Fig. 8. The average thickness of oxide layers formed on the surface of the alloys: (a) and (c) for Ti-48Al-2Cr-2Mo; (b) and (d) for Ti-48Al-2Cr-2Mo-0.5Si, alloys.

The cross sections of the specimens of alloys obtained after exposure to 700°C have not been presented because of the relatively minor thickness of oxide scale. It was determined from the EDS analysis that the oxide scale was developed on the surface of the alloys composed of an inner mixed TiO₂ + Al₂O₃ layer, an intermediate Al₂O₃ layer, and an outer TiO₂ layer.

Since the titanium was depleted to establish TiO₂ in the outermost layer, an intermediate Al₂O₃ layer is established due to the rise of aluminium activity

Table 5. Chemical compositions (in at %) of oxide scales at marked points in Fig. 6

Points	Element					
	O	Ti	Al	Cr	Mo	Si
1	60.3	39.1	0.4	0.1	0.1	—
2	59.4	38.8	0.5	0.1	0.1	0.1

underneath this layer. Because Al₂O₃ includes lesser defects and paths compared to TiO₂ it is more difficult for the oxygen anions diffuse through this layer [3, 17]. Below the Al₂O₃ layer, there was a mixed layer comprising a non-protective titanium oxide and a non-continuous alumina. The oxide scale structures of the alloys were determined as TiO₂ + Al₂O₃/Al₂O₃/TiO₂ from the bulk of the alloy to its surface, which were prevalent oxides in TiAl alloys.

Because Al₂O₃ is permeable for both O and Ti ions, the inner mixed layer and the outermost TiO₂ layer would continue to develop. It can be seen from Figs. 7a, 7b that the outer TiO₂ layer grows slower than the inner mixed oxide layer. After oxidation of the alloys at 800 and 900°C for 180 h, the values of average thickness of oxide layers are presented in Fig. 8. In order to determine the average oxide layer thickness, SEM images of three different regions were observed for each of the alloys. It was found that the thickness of the oxide scale was significantly affected by this mixed oxide layer due to that the thickness of the mixed oxide layer was rather thick. Furthermore, the thickness of the oxide scales is increased when the oxidation temperature increased from 800 to 900°C. For example, in both alloys, a 3 times increase in thickness of the oxide scale at 900°C compared to the 800°C was observed.

It was found that the thickness of scales formed on the the alloys with Si addition was slightly smaller compared to the case of other alloys. This behavior can be attributed to the larger thickness of the protective alumina layer. Thus, Si can be regarded as a beneficial alloying element. Nonetheless, this Al₂O₃ layer was not adequately protective, since it inhibited neither the inward diffusion of oxygen nor the outward diffusion of titanium ions.

In addition, the measured thickness of the oxide scales was consistent with the results of the weight changes (see Fig. 1). The outermost TiO₂ layers shown in Figs. 7a, 7b are developed by the outward diffusion of titanium ions [18]. Increasing oxidation temperature accelerates the outwards diffusion of titanium

ions and this resulted in that TiO_2 develops faster than 800°C .

CONCLUSIONS

The oxidation of the TiAl-based intermetallic alloys was carried out at $700\text{--}900^\circ\text{C}$ for 180 h in air. The weight change of Ti-48Al-2Cr-2Mo-0.5Si was lower than that of Ti-48Al-2Cr-2Mo during cyclic oxidation at all exposure temperatures. The alloys with Si addition exhibited superior oxidation resistance than the alloys without Si. The activation energy values of Ti-48Al-2Cr-2Mo and Ti-48Al-2Cr-2Mo-0.5Si alloys were 160 and 137 kJ mol^{-1} , respectively.

The composition and structure of the oxide scale formed on the alloys was similar. After exposure at 800 and 900°C , a triple-layered scale developed on the surfaces and consisted of $\text{TiO}_2+\text{Al}_2\text{O}_3/\text{Al}_2\text{O}_3/\text{TiO}_2$ from the bulk of the alloy to its surface.

REFERENCES

1. S. Ye, H. Hao, W. Mo, K. Yu, L. Litao, C. Deng, and P. Yu, "Effects of cold compacting pressure on the expansion behavior of Ti-48Al during sintering," *J. Alloy Compd.* **673**, 399–404 (2016).
2. Z. Zhang, M. Xu, C. Z. Zhang, J. C. Han, Y. F. Chen, F. T. Kong, and Y. Y. Chen, "Microstructure homogeneity and mechanical properties of large-size as-cast high Nb containing TiAl alloy ingot," *Phys. Met. Metallogr.* **119**, 953–960 (2018).
3. Y. Garip and O. Ozdemir, "Comparative study of the oxidation and hot corrosion behaviors of TiAl-Cr intermetallic alloy produced by electric current activated sintering," *J. Alloy Compd.* **780**, 364–377 (2019).
4. A. Banu, M. Marcu, S. Petrescu, N. Ionescu, and A. Paraschiv, "Effect of niobium alloying level on the oxidation behavior of titanium aluminides at 850°C ," *Int. J. Miner., Metall. Mater.* **23**, 1452–1457 (2016).
5. C. Liu, X. Lu, F. Yang, W. Xu, Z. Wang, and X. Qu, "Metal injection moulding of high Nb-containing TiAl alloy and its oxidation behaviour at 900°C ," *Metals* **8**, 1–14 (2018).
6. A. Brotzu, F. Felli, and D. Pilone, "Effect of alloying elements on the behaviour of TiAl-based alloys," *Intermetallics* **54**, 176–180 (2014).
7. D. J. Kim, D. Y. Seo, H. Saari, T. Sawatzky, and Y.-W. Kim, "Isothermal oxidation behavior of powder metallurgy beta gamma TiAl-2Nb-2Mo alloy," *Intermetallics* **19**, 1509–1516 (2011).
8. S. Grasso, Y. Sakka, and G. Maizza, "Electric current activated/assisted sintering (ECAS): a review of patents 1906–2008," *Sci. Technol. Adv. Mater.* **10**, 1–24 (2009).
9. Y. Garip and O. Ozdemir, "Hot corrosion behavior of Ti-48Al and Ti-48Al-2Cr intermetallic alloys produced by electric current activated sintering," *Metall. Mater. Trans. A* **49**, 2455–2462 (2018).
10. R. Orru, R. Licheri, A. M. Locci, A. Cincotti, and G. Cao, "Consolidation/synthesis of materials by electric current activated/assisted sintering," *Mater. Sci. Eng., R* **63**, 127–287 (2009).
11. D.-B. Lee, "Effect of Cr, Nb, Mn, V, W and Si on high temperature oxidation of TiAl alloys," *Met. Mater. Int.* **11**, 141–147 (2005).
12. Y. Shida and H. Anada, "The effect of various ternary additives on the oxidation behavior of TiAl in high-temperature air," *Oxid. Met.* **45**, 197–219 (1996).
13. H. Li, Q. Cao, and Z. Zhu, "Oxidation behaviour of Super 304H stainless steel in supercritical water," *Corros. Eng., Sci. Technol.* **53**, 293–301 (2008).
14. E. Godlewska, M. Mitoraj, F. Devred, and B. E. Nieuwenhuys, "Reactivity of a Ti-45.9Al-8Nb alloy in air at $700\text{--}900^\circ\text{C}$," *J. Therm. Anal. Calorim.* **88**, 225–230 (2007).
15. D. Y. Seo, T. D. Nguyen, and D. B. Lee, "Oxidation of powder metallurgy (PM) Ti-48% Al-2% Cr-2% Nb-(0–1%) W alloys between 800 and 1000°C in air," *Oxid. Met.* **74**, 145–156 (2010).
16. K. Kothari, R. Radhakrishnan, and N. M. Wereley, "Advances in gamma titanium aluminides and their manufacturing techniques," *Prog. Aeronaut. Sci.* **55**, 1–16 (2012).
17. X. Liu, K. You, Z. Wang, M. Zhang, and Z. He, "Effect of Mo-alloyed layer on oxidation behavior of TiAl-based alloy," *Vacuum* **89**, 209–214 (2013).
18. D. J. Kim, D. Y. Seo, Q. Yang, H. Saari, T. Sawatzky, and Y.-W. Kim, "Isothermal oxidation behaviour of beta gamma powder metallurgy TiAl-4Nb-3Mn alloys," *Can. Metall. Q.* **50**, 416–424 (2011).